Journal of the Australian Ceramic Society
https://doi.org/10.1007/s41779-024-01068-w

RESEARCH

Ytterbium-doping contribution to the overall dielectric and electrical properties of (Sr, Ba)$Bi_2Ta_2O_9$ ceramics

Mohamed Afqir[1] · Didier Fasquelle[2] · Amina Tachafine[2] · Yingzhi Meng[3] · Mohamed Elaatmani[1] · Abdelouahad Zegzouti[1] · Mohamed Daoud[1]

Received: 25 August 2023 / Revised: 23 June 2024 / Accepted: 21 July 2024

Abstract
In this work, Yb-doped $Sr_{0.95}Ba_{0.05}Bi_2Ta_2O_9$ powders were synthesized by the citric acid-assisted method. The prepared powders were uniaxially pressed and sintered at different temperatures. Structure, morphology, and dielectric properties were investigated. The use of either a 1200 °C sintering temperature or motifs for a reduction tanδ purpose. The results showed that Yb has not caused a significant change in dielectric properties at low temperatures, thus indicating its ability to reduce dielectric loss smoothly. At high temperatures, the introduction of ytterbium elements could reduce both Curie temperature and conductivity. According to Jonscher's universal power law, the correlated barrier-hopping (CBH) model describes the AC conductivity mechanism. However, the non-overlapping small polaron tunneling (NSPT) model may be used to show that this is only possible at a specific temperature. The Arrhenius law and the CBH module provide estimates of the various energy barriers that space charges should overcome; however, these barriers get higher as the dopant concentration rises.

Keywords Dielectric · Conductivity · Electrical modulus · Sintering

Introduction

$SrBi_2Ta_2O_9$ and doped materials that have semiconductor properties have received attention in photocatalytic applications [1, 2]. Substitution at the Sr-site, Ta-site, or both are mentioned as recommended sites for improving ferroelectric properties [3]. Thus, rare earth-doped $SrBi_2Ta_2O_9$ (rare earth elements: Y, Eu, and Sm) compounds were prepared by the solid-state reaction method and analyzed the influence of dopant concentration on the optical and dielectric properties. $SrBi_2Ta_2O_9$ containing rare-earth exhibits low-dielectric loss and involves, technologically, a potential candidate for w-LED [4–6]. The sintering process and doping level are common challenges $SrBi_2Ta_2O_9$ faces when trying to enhance dielectric properties. In this regard, tremendous research is conducted regarding sintering temperature and the doping amount that should have been used to enhance physical properties [7–9]. Thus, introducing motifs into the lattice structure leads to local disorders of unit cells, while the stirring process welds the grains, leading to well-maintained and dense ceramics. A significant difficulty has continued to be the tunability of lowering dielectric loss. The hybridization of Bi (6s) and O (2p) at the band edge position is a general feature of the Aurivillius phases, which means that structural tailoring at Bi^{3+} sites would affect the electrical behavior. Aurivillius phases are mostly displacive-type ferroelectrics. In the case of $SrBi_2Ta_2O_9$ and $SrBi_2Nb_2O_9$ ceramics, this dopant significantly enhanced both the dielectric characteristics and the quality of the ceramics.

Prior research suggests that rare earth substitution at the Sr-site enhances the remanent polarization without sacrificing other physical properties. In contrast, the research conducted on the substitution of Sr with rare earth elements was shifted toward [10–12]. In contrast,

✉ Mohamed Afqir
mohamed.afqir@yahoo.fr

[1] Laboratoire des Sciences des Matériaux et optimisation des procédés, Faculté des Sciences Semlalia, Université Cadi Ayyad, Marrakech, Maroc

[2] Unité de Dynamique et Structure des Matériaux Moléculaires, Université du Littoral Côte d'Opale, Calais, France

[3] Guilin University of Technology, Guilin 541006, China

Published online: 01 August 2024

the research conducted on the substitution of Bi by rare earth elements shifted mainly toward luminescence properties [14]. Scarce research has been done on trivalent rare earth ion doping at the Bi^{3+} site to further investigate the electrical and dielectric properties [15]. In this regard, this work brings out two points. The first point sheds light on methodology and structural characterization. The extent of the effect of motifs on electrical properties is discussed in the second point.

Experimental

The raw materials, made up of $SrCO_3$ (Riedel-de Haën), $BaCO_3$ (Panreac), Bi_2O_3 (RECTAPUR), Yb_2O_3 and Ta_2O_5, were weighed stoichiometrically and mixed with citric acid (Riedel-de Haën) for 30 min. The mixture was initially heated for 6 h at 500 °C. After that, the obtained powder was ground and then calcined for eight hours at 1100 °C.

XRD (Rigaku) technique was performed to track the transformation of reactants into desired products. The XRD patterns were recorded for 2θ values in a range of 10–70 with a step of 5°/min.

Paste electrodes were fixed on both surfaces of the sintered pellets and fired at 400 °C for 20 min in air. Dielectric measurements were carried out using the Solartron 1260 impedance/gain-phase analyzer and Agilent 4294 A.

Results and discussion

Figure1 gives XRD patterns of Yb-doped $Sr_{0.95}Ba_{0.05}Bi_2Ta_2O_9$ compounds. All prepared compounds matched the $SrBi_2Ta_2O_9$ standard reference one (PDF#01-089-6490). The intensitest peak refers to Miller indices (115) which characterizes bismuth layer-structured with two octahedral layers in the perovskite slab [16].

However, for x = 0.2 (3.44 at%) sample, the extra peaks appeared due presumably to the residual impurities emanating from unreacted precursors during synthesis. As a result, it could not be feasible to introduce into a unit cell more than 1.71 at% of motifs.

Figure 2-(a) compares the lattice constants across different synthesized compounds. Overall, the average crystallite size dropped, however, the micro-strain increased when the Yb amount increased. For the unpoled sample, the crystallite size was 55.6 nm, however, this value had dropped to 39.9 nm for the x = 0.1 sample. On the other hand, the microstrain was nearly 0.19% in the undoped sample, which rose slightly to 0.27% for x = 0.1 sample. The three lines of Fig. 2-(b) give the lattice parameters a, b and c as a function of Yb amount, and the inset table compares their cell volume. It is clearly seen from the table, the dopant lowered the unit cell volume. As seen from the graph, both lattice constants "c" and "b" were shifted differently, so that if one is increased while the other is decreased. However, a decrease was noticed for the lattice constant "a". For all

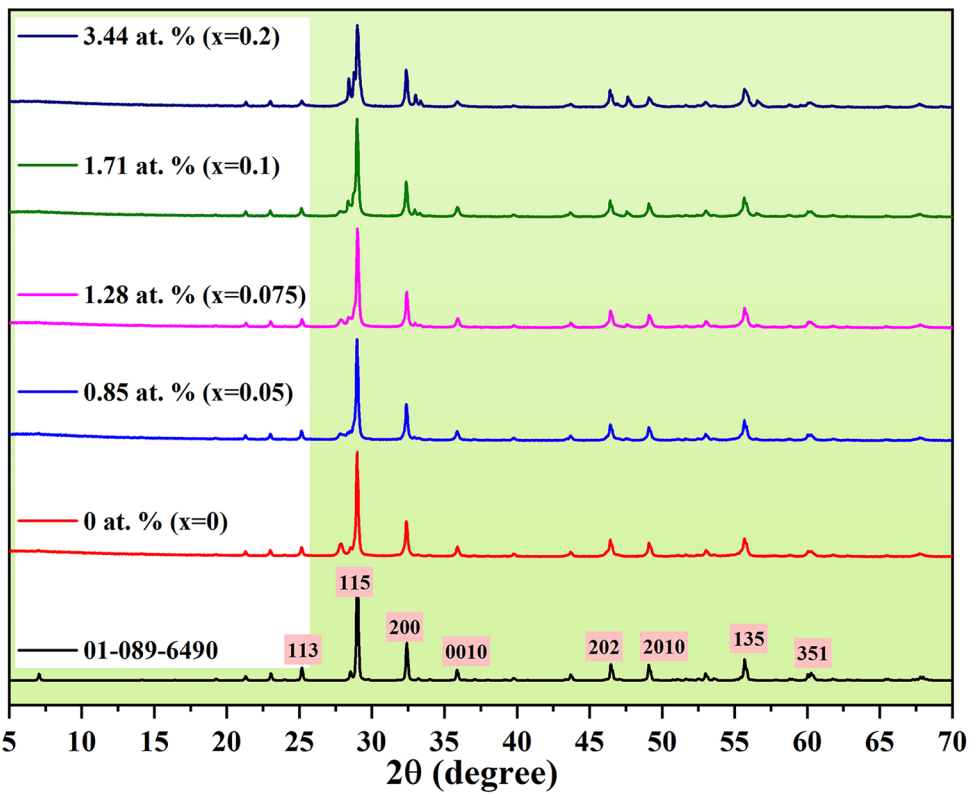

Fig. 1 XRD patterns of Yb-doped $Sr_{0.95}Ba_{0.05}Bi_2Ta_2O_9$

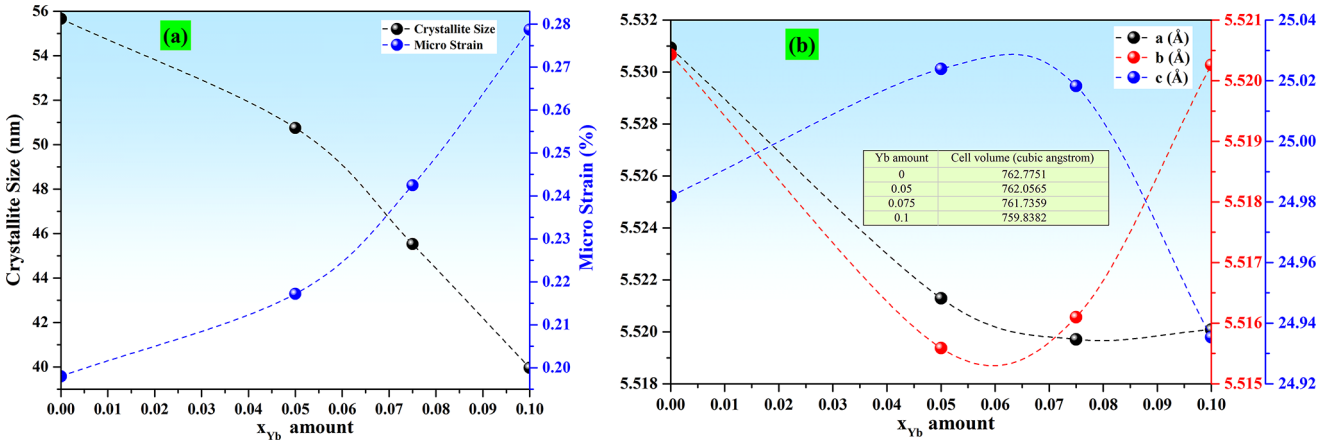

Fig. 2 (a) Crystallite size, micro-strain and (b) lattice constants of Yb-doped $Sr_{0.95}Ba_{0.05}Bi_2Ta_2O_9$

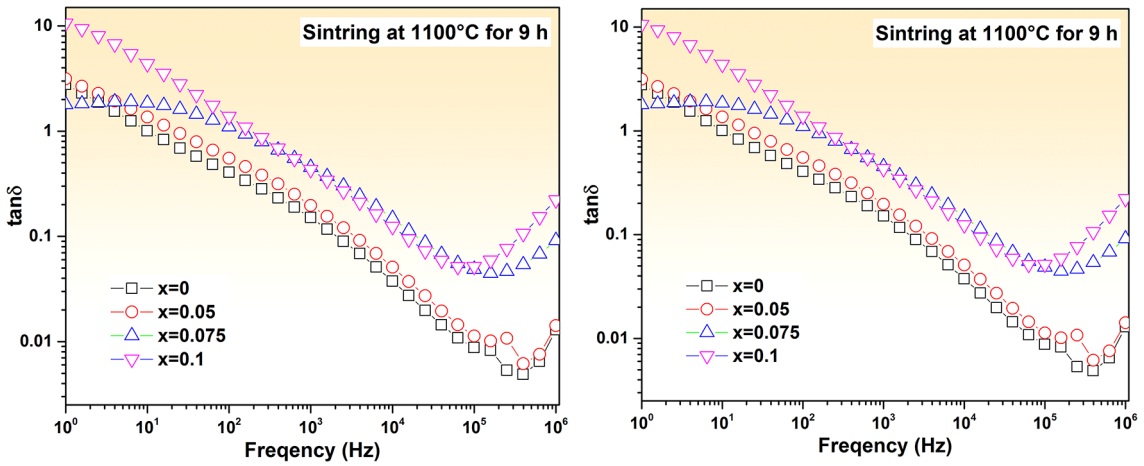

Fig. 3 Effect of sintering temperature on dielectric loss for Yb-doped $Sr_{0.95}Ba_{0.05}Bi_2Ta_2O_9$ ceramics

of those reasons, this leads directly to the consideration that the incorporation of dopants into the lattice structure may result in a change of unit cell.

The effect of sintering temperature on dielectric loss versus frequency measured at room temperature for Yb-doped $Sr_{0.95}Ba_{0.05}Bi_2Ta_2O_9$ ceramics is reported in Fig. 3. Overall, tanδ appears to be temperature dependent, with a difference between doped and undoped samples. Further on, the inability of the dipoles to align themselves in the direction of the electric field causes the tanδ to fall as frequency increases. Meanwhile, the tanδ values are strongly affected by temperature. Thus, at 1 kHz, the figures are 0.15 and 0.03 for undoped samples when measured at 1100 °C and 1200 °C respectively. As well as for the x = 0.1 sample, the tanδ is found to be 0.4 and 0.04 for 1100 °C and 1200 °C respectively. As a result, the higher the sintering temperature, the more grains are welled and porous are removed, resulting in lower dielectric loss. At 1200 °C, the tanδ value is reduced from 0.03 to 0.008 as the amount of ytterbium is increased from x = 0 to x = 0.1, when measured at 1 kHz. Thus, Yb-doping reduces smoothly dielectric loss either because the valence of rare earth is the same as Bi^{3+}.

The Fig. 4 shows the dielectric constant (ε') and dielectric loss (tanδ) for Yb-doped $Sr_{0.95}Ba_{0.05}Bi_2Ta_2O_9$ sintered at 1200°C as a function of temperature and frequency. From room temperature to 200°C, the dielectric constant changes smoothly depending on frequency. By 260°C, the dielectric constant increases significantly and peaked at 330, 288, 284, and 280 for x = 0, 0.05, 0.075, and 0.1, respectively. These figures show that ε' decreases with Yb-doping level at Curie temperature from 121.35 for an undoped sample to 882.13, 956.96 and 868.08 for x = 0.05, 0.075 and 0.1 samples respectively. This might be explained not only by the fact that motifs that were introduced into the lattice structure involve local distortion in the unit cell, but also the contribution of lone pair bismuth.

In the inset tanδ-graphs, all compounds exhibit the lowest tanδ ranging from 0.03 to 0.04, when measured in the room temperature–260 °C range. However, by 260 °C, there is a dramatic rise in tanδ values.

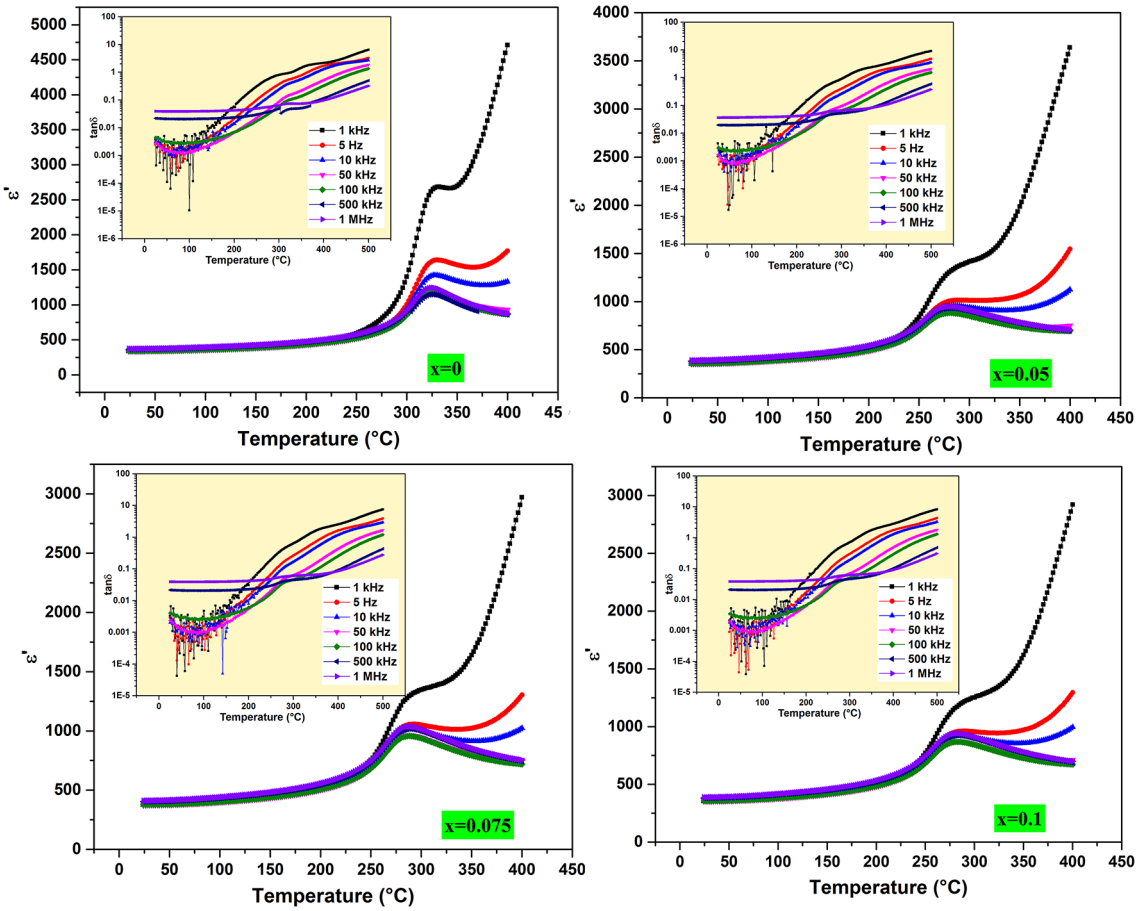

Fig. 4 Dielectric constant (ε') and dielectric loss (inset graph) versus both frequency and temperature for Yb-doped $Sr_{0.95}Ba_{0.05}Bi_2Ta_2O_9$ ceramics

The AC conductivity variation, illustrated in Fig. 5, exhibits a plateau region, which appeared in the low frequency region, and a frequency-dependent region. As the temperature rises, the AC conductivity increases; this behavior is a characteristic of the negative temperature coefficient of resistance property. The effect of Yb-doping is substantially observed at high frequencies (> 10 kHz). Thus, at 107226.7 Hz, the AC conductivity value for an undoped sample is $7.88*10^{-4}$ S/m, which is reduced to 6.710^{-4} S/m, 5.810^{-4} S/m, and 4.9810^{-4} S/m for x = 0.05, 0.075 and 0.1, respectively, when measured at 350 °C. The curves may be described by Jonscher's law.

$$\sigma_{ac} = \sigma_{dc} + A\omega^{s}$$

where σ_{dc}, A and s are dc conductivity, temperature independent pre-exponential factor and frequency exponent respectively. The exponent factor "s" versus temperature reported in the inset graph is not only less than 1 but also decreases with increasing temperature, bringing out the correlated barrier hopping model as one of the most appropriate models to explain the conduction mechanism in these compounds within the 350–450 °C temperature range [17]. However, at a certain temperature, the s values rise as the temperature rises, indicating the possibility of a non-overlapping small polaron tunneling (NSPT) process [18].

In the CBH process, the frequency exponent could be simplified into.

$$s \approx 1 - \frac{6k_BT}{W_M}$$

where k_B and W_M are Boltzmann's constant and potential barrier over which the charge carriers must hop respectively. The W_M values for x = 0, 0.05, 0.075, and 0.1, respectively, are 0.14, 0.29, 0.35, and 0.24 eV using linear fitting with a negative slope region of s-T plots. When, ytterbium atoms are brought into the lattice structure, this barrier potential (W_M) is decreased.

Using the maximum value of the potential barrier's height (W_M), the distance (R_ω) of the jump between the two neighboring wells can be calculated.

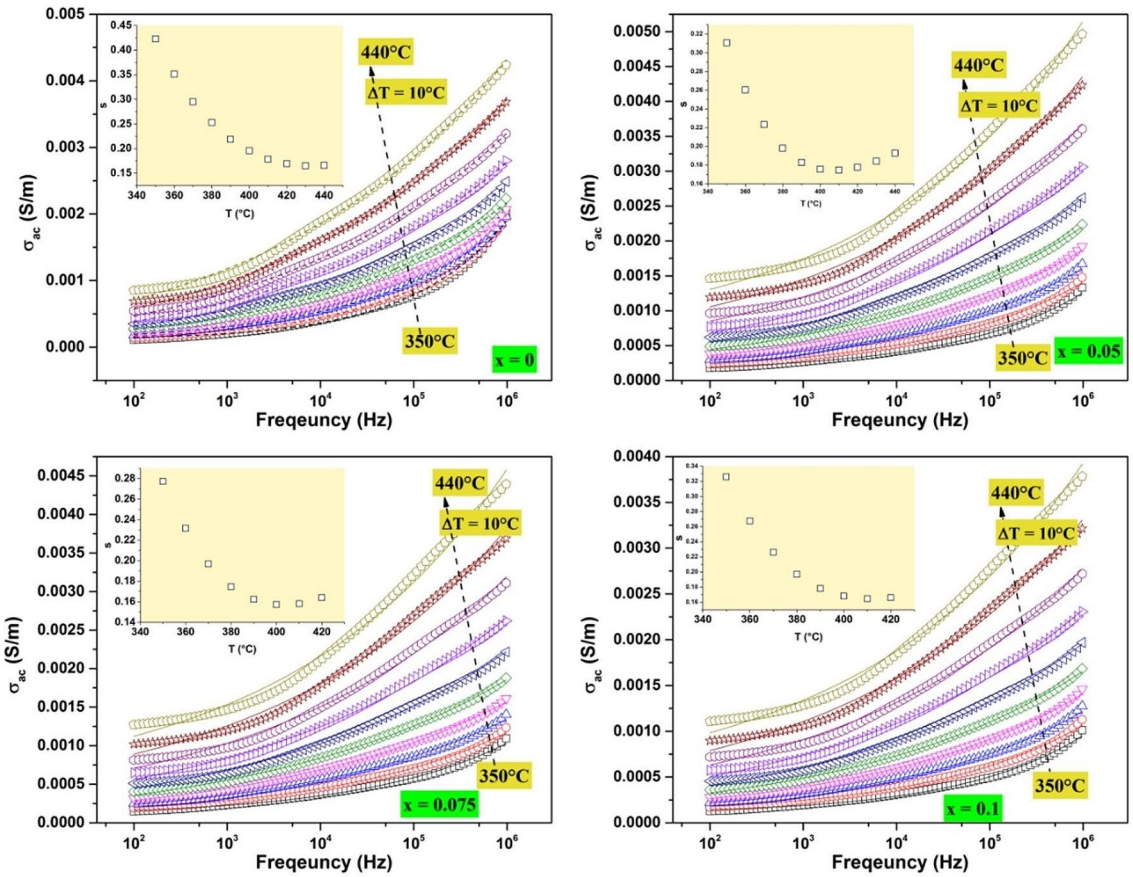

Fig. 5 Temperature and frequency dependence of Yb-doped $Sr_{0.95}Ba_{0.05}Bi_2Ta_2O_9$ ceramics

$$R_\omega = \frac{e^2}{\pi \in' \in_0 \left[W_M - k_B T \mathrm{Ln}\left(\frac{1}{\omega\tau_0}\right)\right]}$$

In this equation, e is the charge of electron, ε′ is the dielectric constant, ε_0 is the permittivity of free space, k_B is the Boltzmann constant, ω is the angular frequency, and τ_0 is the characteristic relaxation (10^{-12} s). Figure 6 illustrates how the R_ω of all synthesized compounds is frequency dependent at various temperatures. At low frequency [100–284.8 Hz], while the R_ω increases with frequency, it drops as the temperature rises. However, at high frequency [343046.9–977010 Hz], with rising temperature and frequency, the R_ω rises only for the undoped sample. However, for samples that have been doped, the R_ω rises as the temperature rises until it reaches a certain temperature, at which point it falls.

As a result, the charge carrier density rises as a result of the reduction in hopping distances, which also causes a rise in AC conductivity. Dopant, on the other hand, is found to increase R_ω at fixed temperatures and frequencies; for example, at 225.7 Hz and 360 °C, the R_ω increases from $6.52*10^{-3}$Å for an undoped sample to $9.22*10^{-3}$Å for x = 0.1 sample.

The Nyquist (Z′-Z″) plots measured at different temperatures for Yb-doped $Sr_{0.95}Ba_{0.05}Bi_2Ta_2O_9$ compounds are given in Fig. 7. All compounds exhibit two overlapped semicircles' arcs arising from grain and bond grain boundaries. Meanwhile, as the temperature increases, the radius of semicircles' arcs diminishes.

An analogous circuit that consists of a series of two subcircuits, one of which represents a grain effect and the other a grain boundary, was used to fit the Nyquist plot. In order to get grain resistance (R_g), as well as grain-boundary resistance (R_{gb}), a set of points with a constrained radius were fitted into a circle at 440 °C. The estimated R_g is found to be around 6.47, 7.13, and 7.90 kΩ for x = 0.05, 0.075, and 0.1, respectively, which is slightly larger than the one estimated for the undoped sample (R_g = 5.73 kΩ). However, the grain boundary resistance decreased from 23.40 kΩ for the undoped sample to 16.12, 19.74, and 22.42 kΩ for x = 0.05, 0.075, and 0.1 samples, respectively. What should be clear from these R_g and R_{gb} values is that grain-boundary contributions outweigh grain ones on the one hand, and on the other hand, doping enhanced grain resistance.

The AC conductivity versus temperature at different frequencies are reported in Fig. 8. Firstly, the AC conductivity

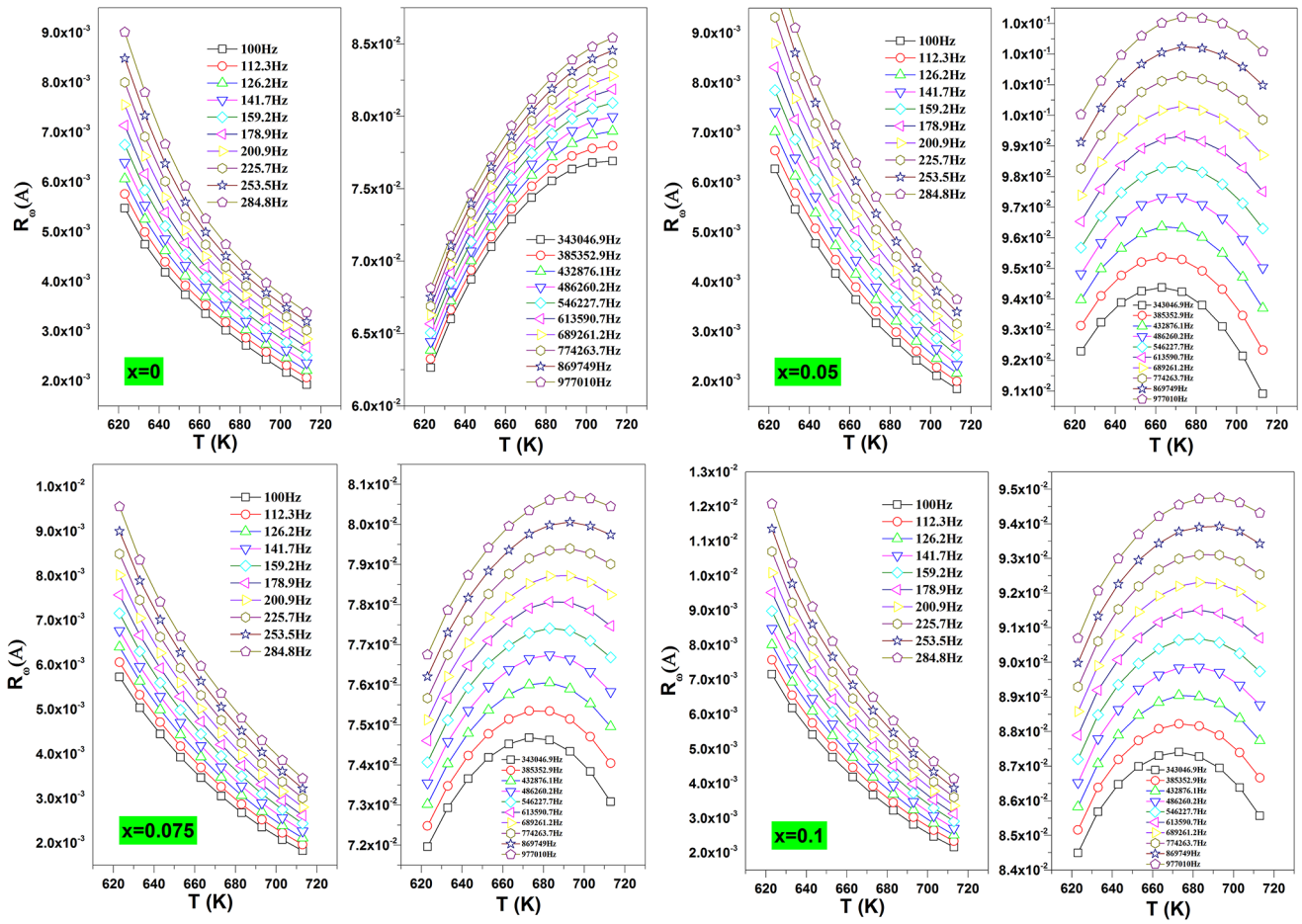

Fig. 6 Temperature and frequency-dependence of hopping distance

depends only on frequency, considering the low temperature. Above 260 °C, it starts increasing linearly with increasing temperature. In the set graph, the Arrhenius law is used to estimate activation energy within the 350–440 °C range.

$$\sigma_{ac} = \sigma_0 e^{\frac{-Ea}{k_B T}}$$

where σ_0, k_B and E'_a are constants, Boltzmann's constant and activation energy respectively. The obtained values are 1.52, 1.72, 1.71 and 1.75 eV for x = 0, 0.05, 0.075, 0.1 samples respectively. the x = 0 exhibits the highest activation energy as well as x = 0.05 and x = 0.075 samples. However, the undoped sample has the lowest E_a value. As a result, the more activation energy is higher, the more carrier charge mobility is hampered. Thus, the AC conductivity, obtained from the set graph at 350 °C, decreases from $4.23*10^{-4}$ S/m form the undoped compound to $3.69*10^{-4}$ and $3.10*10^{-4}$ S/m for x = 0.075 and x = 0.1 respectively.

Frequency-dependent electrical modulus at different temperatures for each compound is given in Fig. 9. M' curves can be modeled as an S-shaped function that imposes a saturation level in the higher frequency region. M" curves are composed of two relaxation processes that appear at low and high frequencies. These asymmetric broadening peaks are frequency-independent when the temperature is increased.

The top (M'_{max}) to bottom (M'_{min}) M'-curve gives the height ΔM' as illustrated in Fig. 9.

$$\Delta M' = M'_{max} - M'_{min}$$

A S-curve typically consists of three parts. The initial period generally tends to be zero. The ramp period is followed by the saturation one. Through Fig. 9, the higher the temperature, the more mobile the carrier charge is. Through Fig. 10-(b), Yb-doping allows widening the gap between M'_{max} and M'_{min} levels. It is obvious that the height of the doped sample is significantly higher than that of the pure sample. However, x = 0.075 and x = 0.1 samples have similar height ΔM'.

A change in the height ΔM' implies a rearrangement of carrier charges. If the height ΔM' is smaller, then the duration of mobility of carrier charges will increase, leading to increased conductivity.

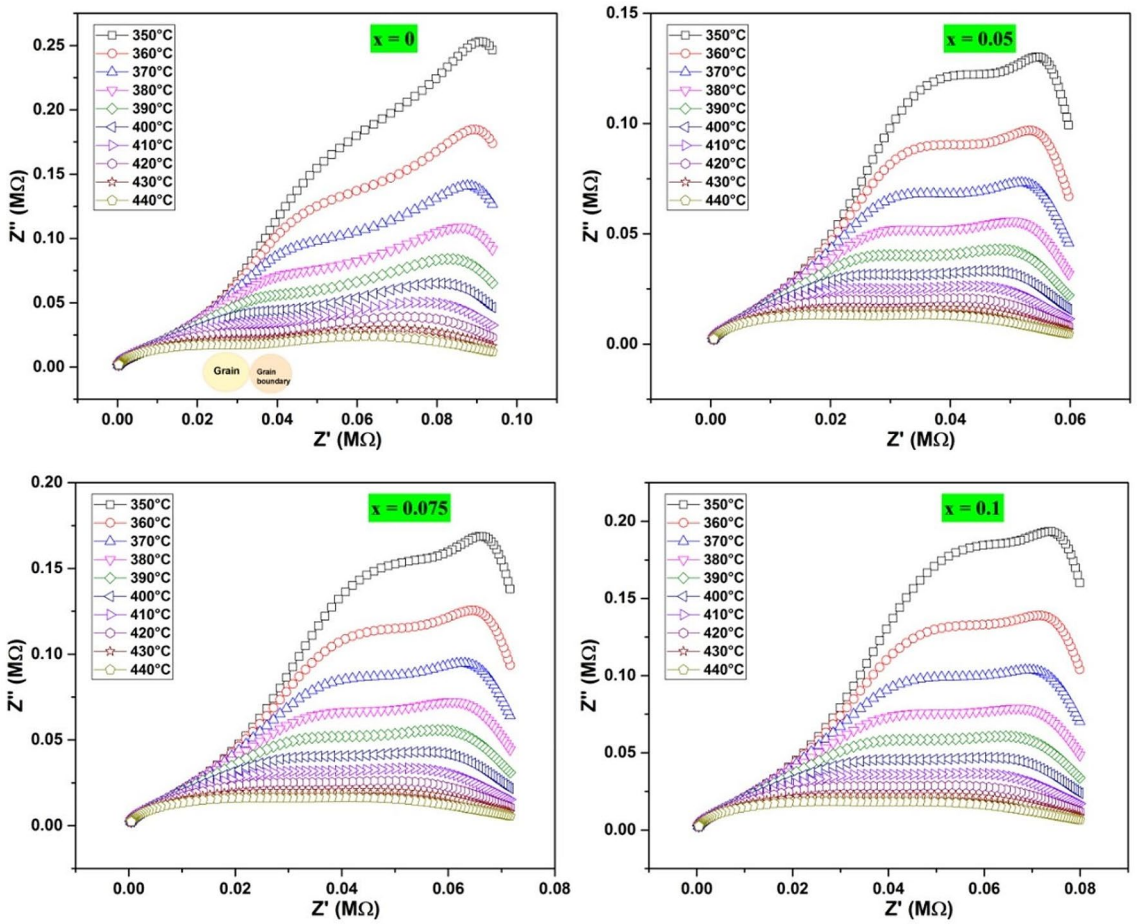

Fig. 7 Nyquist plot of Yb-doped $Sr_{0.95}Ba_{0.05}Bi_2Ta_2O_9$ ceramics

The Arrhenius law is tailor-made for the maximum M" frequency (f_{max}).

$$f_{max} = f_0 e^{\frac{-E'_a}{k_B T}}$$

where f_0, k_B and E'_a are the pre-exponential factor, Boltzmann's constant and activation energy respectively. The linear fitting of this equation allows for getting activation energy values as illustrated in Fig. 10-(a). The activation energy, summarized in Fig. 10-(a), is increased with increasing Yb doping, i.e., from 1.96 eV (x = 0) to 2.27 eV (x = 0.1). As a result, the transition from long-distance to short-distance mobility among doped samples requires more energy to cross potential barrier.

Both activation energy values, estimated either from σ_{ac} versus temperature or fmax versus temperature, have similar evolution as a function of Yb-doping. As a consequence, the carriers' charges might arise from one source. Significantly, the volatilization of bismuth in $SrBi_2Ta_2O_9$ ceramic caused oxygen vacancies [12, 19], which decreased activation energy and increased AC conductivity at high temperatures. The high activation energy value is mostly due to the suppression of lattice oxygen species in the framework. The contribution of the polaron is strengthened, however, by the parameters R_ω and binding energy W_M calculated from the CBH process. Therefore, the Coulomb barrier separating two defect centers is crossed by a single polaron or a bipolaron during the conduction process [20, 21].

Conclusion

Through the citric acid-assisted method, it could be possible to synthesize compounds with the required purity. All compounds exhibit a similar crystal structure to that of $SrBi_2Ta_2O_9$, but the motifs bring into the lattice structure a smooth distortion, which is revealed by the XRD technique.

1200 °C remains an ideal sintering temperature for densifying ceramics, thus lowering dielectric loss. However, at room temperature, double replacement taking place on both the Sr and Bi in the lattice structure may not substantially affect dielectric loss.

Electrical and dielectric results could be split into two parts. From room temperature to 206 °C, dielectric and

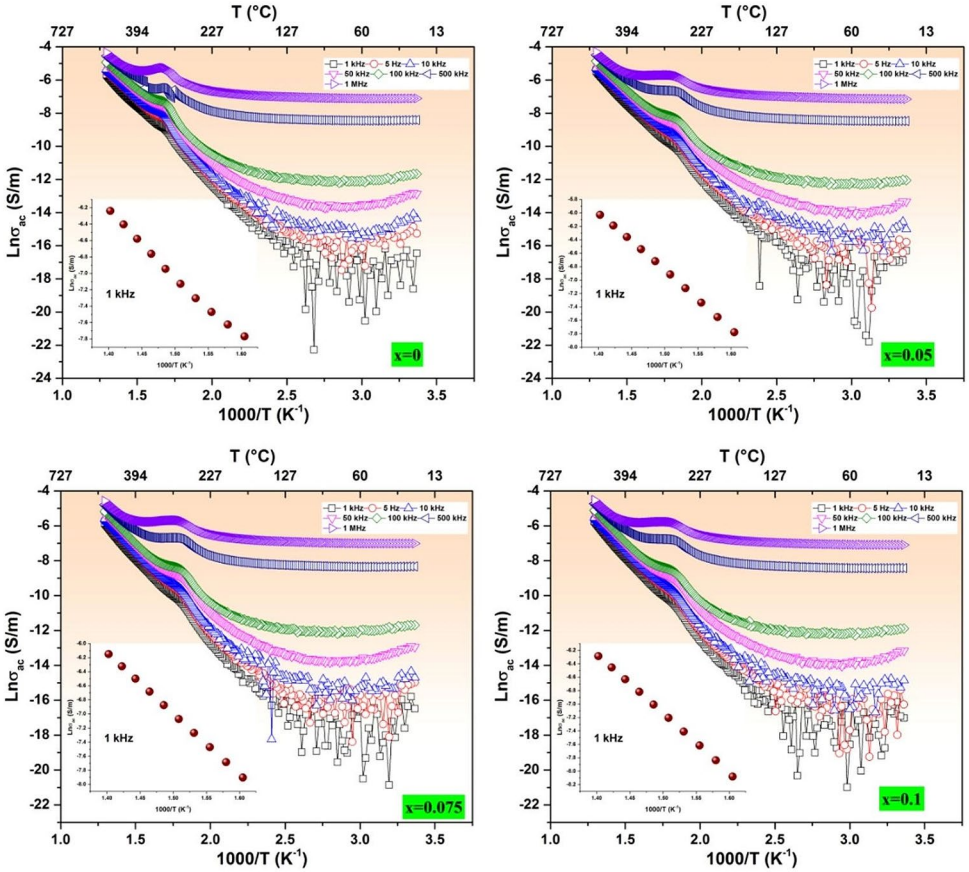

Fig. 8 AC conductivity versus temperature at different frequencies of Yb-doped $Sr_{0.95}Ba_{0.05}Bi_2Ta_2O_9$ ceramics

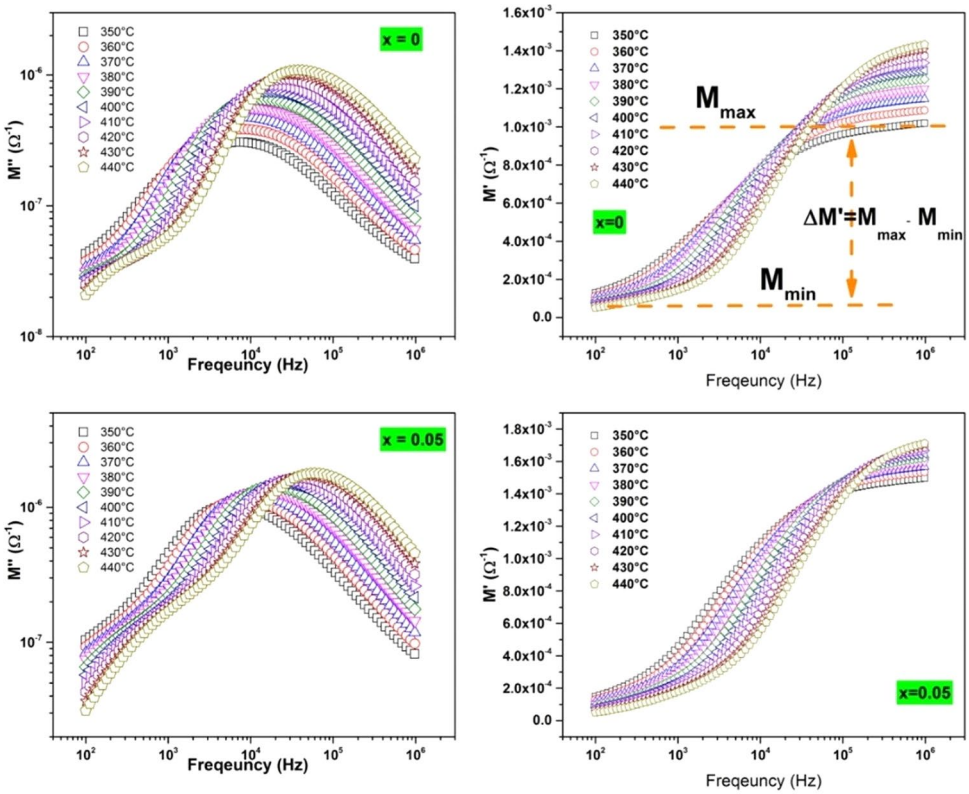

Fig. 9 Frequency-dependent electrical modulus at different temperatures of Yb-doped $Sr_{0.95}Ba_{0.05}Bi_2Ta_2O_9$ ceramics

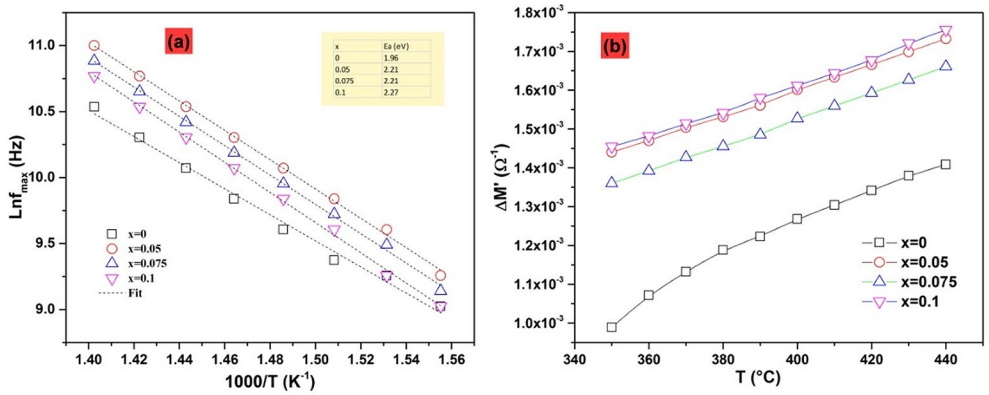

Fig. 10 (a) Arrhenius plot of maximum frequency from electrical modulus M". (b) height s-curve from electrical modulus M'

electric properties do not shift significantly when Yb atoms are brought into the structure. However, the effect of doping appears beyond 260 °C. Thus, doping lowers both conductivity and the Curie temperature.

Hopping-level conduction in samples was analyzed using the correlated barrier hopping model. The conductivity may also be affected by two processes, one of which is relevant and results from oxygen vacancies and the other from polaron hopping.

Authors' contributions All authors approved the final manuscript.

Funding No funding was received.

Data availability All data generated or analyzed during this study are included in this article. Requests for material should be made to the corresponding author (Mohamed AFQIR).

Declarations

Statement Regarding Research Involving Human Participants and/or Animals The presented work has nothing to do with human participants and/or animals.

Competing interests The authors declare that they have no competing interests.

References

1. Liao, B., Liao, X., Xie, H., Qin, Y., Zhu, Y., Yu, Y., Hou, S., Zhang, Y., Fan, X.: J. Mater. Sci. Technol. **123**, 222 (2022)
2. Li, N., Zhu, Q., Liu, G., Zhao, Q., Lv, H., Yuan, M., Meng, Q., Zhou, Y., Xu, J., Wang, C.: J. Mater. Sci. Technol. **122**, 91 (2022)
3. Wendari, T.P., Ikhram, M., Putri, Y.E., Septiani, U.: Ceram. Int. **48**, 10328 (2022)
4. Zhong, Y., Deng, B., Gao, X., Sun, P., Ren, Y., Liang, T., Yu, R.: J. Lumin. **215**, 116648 (2019)
5. Senthil, V., Badapanda, T., Panigrahi, S.: AIP Conf. Proc. 2115, (2019)
6. Senthil, V., Badapanda, T., Bose, A.C., Panigrahi, S.: J. Mater. Sci. Mater. Electron. **27**, 1602 (2016)
7. Lu, C.H., Huang, Y.H.: Adv. Appl. Ceram. **107**, 305 (2008)
8. Li, B., Li, L., Wang, X.: Ceram. Int. **29**, 351 (2003)
9. Lu, C.H., Chen, Y.C.: J. Eur. Ceram. Soc. **19**, 2909 (1999)
10. Noguchi, Y., Miyayama, M., Oikawa, K., Kamiyama, T.: J. Appl. Phys. **95**, 4261 (2004)
11. Noguchi, Y., Kitamura, A., Woo, L.C., Miyayama, M., Oikawa, K., Kamiyama, T.: J. Appl. Phys. **94**, 6749 (2003)
12. Miyayama, M., Noguchi, Y.: J. Eur. Ceram. Soc. **25**, 2477 (2005)
13. Zhong, Y., Sun, P., Gao, X., Liu, Q., Huang, S., Liu, B., Deng, B., Yu, R.: J. Lumin. **212**, 45 (2019)
14. Senthil, V., Panigrahi, S.: Int. J. Hydrogen Energy. **44**, 18058 (2019)
15. Zhu, M., Liao, B., Tang, Y., Chen, X., Ma, R., Li, L., Fan, X.: Appl. Surf. Sci. **628**, 157366 (2023)
16. Zhou, Z., Dong, X., Huang, S., Yan, H.: J. Am. Ceram. Soc. **89**, 2939 (2006)
17. Rached, A., Wederni, M.A., Belkahla, A., Dhahri, J., Khirouni, K., Alaya, S., Martín-, R.J.: Phys. B Condens. Matter. **596**, 412343 (2020). Contents
18. Biswas, D., Das, A.S., Mondal, R., Banerjee, A., Dutta, A., Kabi, S., Roy, D., Singh, L.S.: J. Phys. Chem. Solids. **144**, 109505 (2020)
19. Wu, Y., Forbess, M.J., Seraji, S., Limmer, S.J., Chou, T.P., Cao, G.: J. Appl. Phys. **89**, 5647 (2001)
20. Ben Taher, Y., Oueslati, A., Maaloul, N.K., Khirouni, K., Gargouri, M.: Appl. Phys. A. **120**, 1537 (2015)
21. Liu, H., Ma, Z., Guo, X., Yao, B., Wang, Y., Liu, Y., Zhang, F., Sun, H.: Ceram. Int. **48**, 14442 (2022)